OPERATIONAL ANALYSIS OF PV INVERTER REACTIVE POWER CONTROL STRATEGIES FOR MICROGRIDS

Mihai BURLACU[1], Valentin NĂVRĂPESCU[2]

The constantly increasing penetration of renewable energy sources triggered an accelerated transformation process for the energy sector worldwide. The photovoltaic (PV) industry, with applications from the residential sector up to large-scale photovoltaic power plants (PVPPs), was amongst the fasted growing industries. Recently, PVs were integrated in the reactive power control which represents a major component of the microgrids' resources management, aiming at assuring optimal operating conditions. This paper investigates different reactive power control strategies for the PVPPs within a medium voltage microgrid. An operational analysis for a one-year period is conducted to select the most efficient reactive power control strategy.

Keywords: photovoltaic power plant, photovoltaic inverter, reactive power control, microgrids, load flow analysis

1. Introduction

The coordinated measures recently applied to limit climate changes triggered an accelerated transformation process for the energy sector worldwide. The commissioning of new generation capacities based on renewable energy sources, such as wind and solar, represents a major contribution to reducing emissions. The photovoltaic (PV) industry was amongst the fasted growing industries with a 35-40% annual market growth rate [1]. The large-scale and medium-scale photovoltaic power plants (PVPPs) are connected to the transmission or distribution networks, while the small-scale PVs are used in residential applications. The high penetration of medium-scale PVPPs within medium voltage (MV) networks initiated a paradigm shift towards a decentralized operation model. In this purpose, the microgrid concept was introduced as "a group of interconnected loads and distributed energy resources with clearly defined electrical boundaries that acts as a single controllable entity with respect to the grid and can connect and disconnect from the grid to enable it to operate in both grid-connected and island modes" [2]. The microgrids popularity is

[1] PhD Student, Faculty of Electrical Engineering, University POLITEHNICA of Bucharest, Romania, e-mail: mihai.valeriu.burlac@gmail.com

[2] Prof., Faculty of Electrical Engineering, University POLITEHNICA of Bucharest, Romania, e-mail: valentin.navrapescu@upb.ro

constantly increasing, as a performant coordination of local resources has the potential for improving both operational conditions and efficiency. Reactive power control plays a crucial role in assuring optimal microgrid operational conditions [3]. Although initially, PV inverters were required to operate at unity power factor, the current requirements include reactive power support and different strategies are investigated in the literature [4].

This paper aims to investigate different reactive power control strategies for the PVPPs within a medium voltage microgrid. For this purpose, an operational analysis is performed for an entire year in order to select the most efficient reactive power control strategy in terms of reducing the active power losses.

2. Load flow

The load flow (LF) computation is a fundamental calculation performed for power systems in order to determine the steady-state variables such as bus voltage magnitude and angle, active and reactive power flow through the branches. The Backward-Forward Sweep method (BFSM) represents the most appropriate procedure for performing load flow calculation on distribution systems, as it has been developed considering the distribution systems characteristics such as radial or tree-like topologies and low X/R ratio [5]. BFS delivers better convergence and faster computational times than other popular methods such as Newton-Raphson or Fast-Decoupled methods [6].

The BFSM consists in an iterative process, with two main computational steps: (1) *the backward sweep*, when the current flows through the network branches are computed starting with the terminal buses and moving towards the source; and (2) *the forward sweep*, when the bus voltages are determined moving from the source bus towards the terminal buses [7]. Before the iterative process begins, all bus voltages $\underline{U}_j$ are initialized with the source bus voltage $\underline{U}_S$.

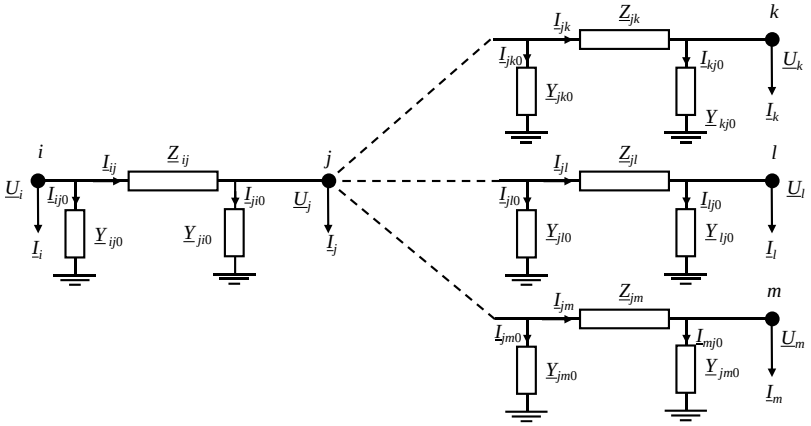

Fig. 1. A generic bus *j*, its predecessor *i*, successors *k*, *l*, *m* and their electrical lines

A generic bus *j* is presented in Fig. 1 together with its predecessor *i* and successors *k, l, m*. The electrical lines are modelled using the Π equivalent circuit, while the loads and distributed generators are modelled as constant active and reactive power absorptions or injections. In Fig. 1, $\underline{U}_j$ is the voltage at bus *j*, $\underline{I}_j$ is the current absorbed from bus *j*, $\underline{I}_{ij}$ is the current through line *i* – *j*, $\underline{Z}_{ij}$, $\underline{Y}_{ij0}$ and $\underline{Y}_{ji0}$ are the impedance and admittances of the *i* – *j* line.

During the backward sweep, the current absorbed from bus *j* and the current through line *i* – *j* are calculated, at iteration *p*, as:

$$\underline{I}_j^{(p)} = \left(\frac{P_{L,j} - P_{G,j} + j\left(Q_{L,j} - Q_{G,j}\right)}{\sqrt{3} \cdot \underline{U}_j^{(p-1)}} \right)^* \tag{1}$$

$$\underline{I}_{ij}^{(p)} = \underline{I}_j^{(p)} + \sum_{k \in Succ(j)} \left(\underline{I}_{jk}^{(p)} + \underline{Y}_{jk0} \cdot \frac{\underline{U}_j^{(p-1)}}{\sqrt{3}} \right) + \underline{Y}_{ji0} \cdot \frac{\underline{U}_j^{(p-1)}}{\sqrt{3}} \tag{2}$$

where $P_{L,j}$, $Q_{L,j}$ and $P_{G,j}$, $Q_{G,j}$ are the active and reactive powers demanded by the loads and supplied by the generators connected at bus *j*.

During the forward sweep, the voltage at bus *j* is computed by:

$$\underline{U}_j^{(p)} = \underline{U}_i^{(p)} - \sqrt{3} \cdot \underline{Z}_{ij} \cdot \underline{I}_{ij}^{(p)} \tag{3}$$

Finally, the apparent power supplied by the source bus $\underline{S}_0$ is calculated:

$$\underline{S}_0^{(p)} = \sqrt{3} \cdot \underline{U}_0 \cdot \left(\sum_{k \in Succ(0)} \underline{I}_{0k}^{(p)} \right)^* \tag{4}$$

The convergence test is performed by comparing the values obtained for $\underline{S}_0$ at two consecutive iterations. If the difference is lower than the admissible error ε, the calculation stops, otherwise a new iteration *p* + 1 is performed:

$$\left| \underline{S}_0^{(p)} - \underline{S}_0^{(p-1)} \right| \le \varepsilon \tag{5}$$

3. PVPP reactive power control strategies

In recent years, as PV penetration is continuously increasing, the reactive power control requirements imposed to the PVPPs are under revision. Initially, the PVPP inverters were required to operate at unity power factor (Fig. 2a), so that no reactive power support was provided to the grid [8].

As PVPP capacities developed, grid operators gradually replaced the requirements, so that the PVPP inverters need to operate at a fixed power factor value cosφ, decided by the distribution system operator (DSO), within a required range [$\cos\varphi_{min}$, $\cos\varphi_{max}$]. In this manner, the PVPPs need to assure a reactive power range [Q_{min}, Q_{max}] proportional to the generated active power P_{gen}, therefore a limited reactive power support is provided at partial power, during the

morning and evening hours (Fig. 2b). In order to overcome these limitations, several DSOs changed the requirements so that the reactive power range, defined at the rated power P_{max}, has to be provided at partial power [9]. The extended reactive power range is presented in Fig. 2c.

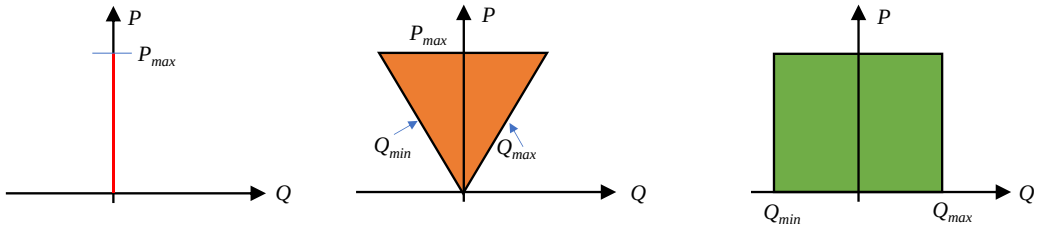

Fig. 2. Required reactive power range for PVPPs operating a) at unity power factor, b) at fixed power factor and c) with extended reactive power range.

Furthermore, a different strategy is considered for medium size PVPPs that are usually connected to the existing MV buses, which already supply other loads. In this case, the inverters' ability to provide local load power factor correction is explored by demanding the PVPPs to fully compensate the reactive power demanded by the local load [10].

Considering the current PVPP reactive power control paradigm, this paper proposes six reactive power control strategies. The first strategy is defined by the PVPP operating at unity power factor, while the PVPPs are operating at a fixed power factor of 0.95, 0.90 and 0.85 under the 2nd, 3rd and 4th strategies. The local load power factor correction is performed under the 5th and 6th strategies, meaning that the PVPP aims at fully compensating the reactive power demanded by the load connected at its Point of Interconnection (POI). The reactive power limits are defined by considering maximum power factor limits applied at P_{gen} for the 5th strategy and at P_{max} for the 6th.

4. Case study

4.1. Microgrid data

The microgrid under study consists of seven different loads such as a hotel, an office building, a school, a mall, a hospital and two residential areas alongside four photovoltaic power plants (PVPP). The microgrid is connected to the MV busbar of a step-down substation by seven MV underground electrical lines, while its tree-like topology, shown in Fig. 3, is inspired by the CIGRE MV benchmark network presented in [11]. The electrical lines parameters are extracted from [12]: resistance r_0 = 0.927 Ω/km, reactance x_0 = 0.142 Ω/km, susceptance b_0 = 47.12389 μS/km, rated current I_{max} = 150 A and power S_{max} = 5196.2 kVA.

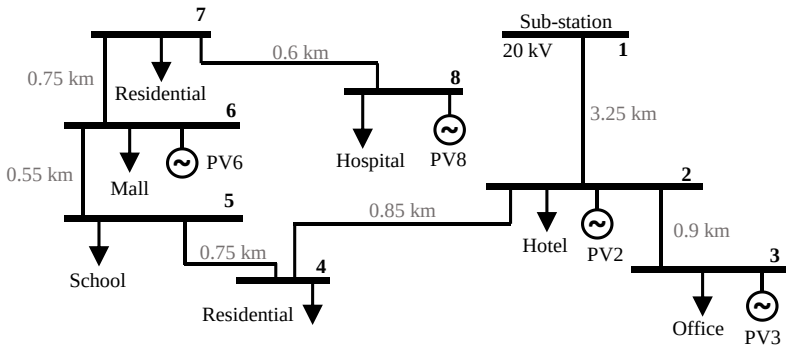

Fig. 3. Microgrid one-line diagram

The load profiles are obtained for each load type from the OpenEI database [13] for an entire year with a one-hour granulation. The maximum, average and minimum demanded active power (P_{max}, P_{avg}, P_{min}) and power factor ($\cos\varphi_i$) values are presented for each load in Table 1. It should be noted that the P_{avg} and P_{min} values are also expressed in percentage relative to P_{max}.

Table 1

Load profiles characteristics

Bus	Type	$P_{max,i}$ [kW]	$\cos\varphi_i$ [-]	$P_{avg,i}$		$P_{min,i}$	
				[kW]	[%]	[kW]	[%]
2	Hotel	265	0.855	136.71	51.6	60.43	22.8
3	Office	710	0.829	243.50	34.3	54.18	7.6
4	Residential	455	0.832	169.84	37.3	51.32	11.3
5	School	405	0.866	125.21	30.9	45.55	11.3
6	Mall	360	0.897	129.40	35.9	11.20	3.1
7	Residential	535	0.851	199.70	37.3	60.34	11.3
8	Hospital	770	0.845	566.62	73.6	286.48	37.2

The PVPP data are presented in Table 2: rated active and apparent power (P_{max}, S_{max}) alongside the minimum and maximum reactive power (Q_{min} , Q_{max}), corresponding to the maximum power factor value $\cos\varphi_{max} = 0.85$ applied at P_{max}. It should also be noted that reactive power injected by the PVPP inverter into the grid is represented by positive values ($Q > 0$). The hourly power output of each PVPPs is obtained from Renewables Ninja database [14], for an entire year.

Table 2

PVPPs rated power and reactive power limits

PVPP	P_{max} [kW]	Q_{min} [kVAr]	Q_{max} [kVAr]	S_{max} [kVA]
PV2	350	–216.9	216.9	411.8
PV3	970	–601.2	601.2	1141.2
PV6	550	–340.9	340.9	647.1
PV8	1150	–700.3	700.3	1329.4

Fig. 4 presents the load profile for each load type and production curve for the PVPPs expressed in percentage relative to P_{max}, for the 20th of May. An

identical production curve is considered for all PVPPs within the microgrid given that they are located relatively close to each other. Also, the same load curve is considered for both residential loads.

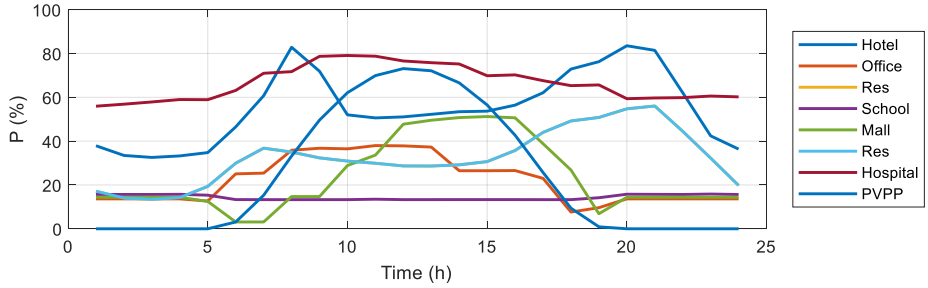

Fig. 4. Load profiles and PV generation curve for the 20th of May

4.2. The Developed Simulation Software

The simulations presented in this paper are performed using a software package developed by the authors under the Matlab Environment. The main module within the software package performs the load flow calculation based on the backward-forward sweep method presented in section 2. The microgrid data, alongside the hourly load and generation curves for the entire year period are imported into the data input module. For each hour, the input data module passes the corresponding data to the load flow computation module. The results are then passed to the post-processing module, which includes functions for performing various analysis based on the results and for generating graphical representations.

The load flow algorithm implemented by the authors is validated by using the Matpower [15] toolbox as reference. The bus voltage absolute errors presented in Table 3 reveal that the errors are lower than 0.085 V, which represents $4.2 \cdot 10^{-6}$ p.u. Also, the error for active and reactive powers supplied by the source are lower than $2.2 \cdot 10^{-5}$ kVA. The results obtained demonstrate that the load flow computation module, implemented by the authors based on the BFS method, provides high accuracy, therefore it will be further utilized for the operational analysis performed in this paper.

Bus Voltage Absolute Errors (V)	Bus 1	Bus 2	Bus 3	Bus 4	Bus 5	Bus 6	Bus 7	Bus 8
	0.000	0.079	0.082	0.024	0.085	0.002	0.032	0.075

4.4. One-day analysis

In this section the operational analysis is conducted for a single day, the 20th of May, characterized by a very high PV generation and an average load demand. The reactive power provided by the four PVPPs in each of the six considered strategies are presented in Fig. 5.

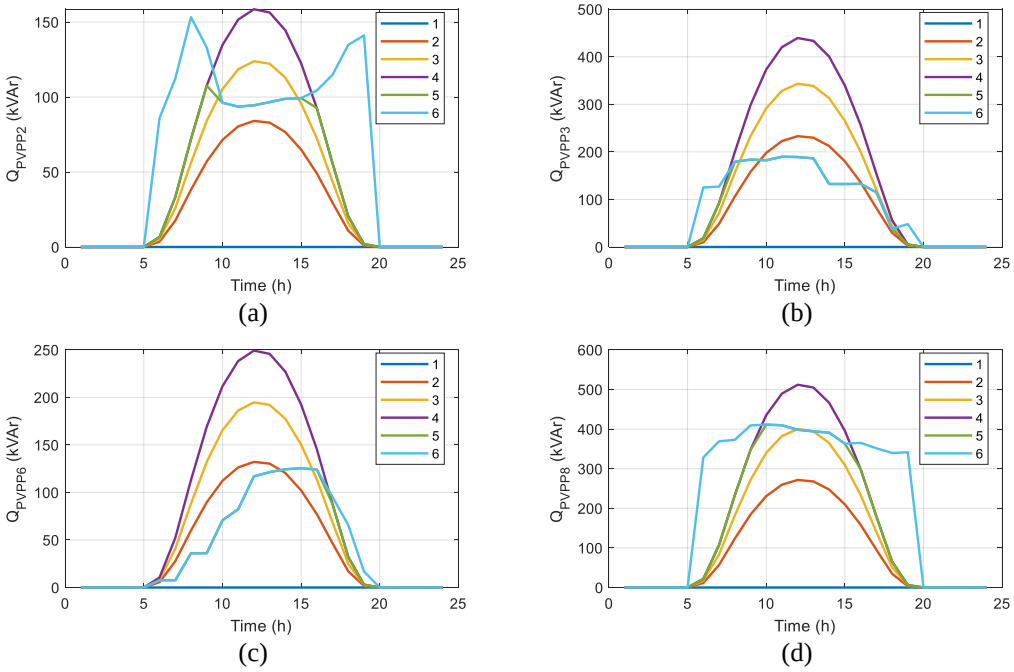

Fig. 5. PVPP reactive power output for the 20th of May under each strategy.

The reactive power demand follows a different profile for each load, therefore operating the PVPPs under the fixed power factor strategies (2nd, 3rd and 4th) provides either a reactive power excess (e.g. the 3rd and 4th strategies during the 12th time interval for the PVPPs at buses 2, 3 and 6) either a deficit (e.g. the 2nd strategy during the entire day for PVPP2 and PVPP8). On the other hand, under the 5th and 6th strategies the PVPPs reactive power output is determined in order to compensate the reactive power demanded by the local loads. The reactive power limits are defined by considering the maximum power factor and the generated active power P_{gen} for the 5th strategy and the rated active power P_{max} for the 6th strategy. In this manner, PVPP3 and PVPP6 are able to completely compensate the reactive power demanded by the office and mall loads during the entire day-light period of the day. However, when the 5th strategy is applied, PVPP2 and PVPP8 are not capable to fully compensate the hotel and hospital, while under the 6th strategy, the extended reactive power limits allow the PVPPs to fully compensate the local loads.

Fig. 6a presents the total active power demanded by all the loads (P_{load}), the total active power generated by the PVPPs (P_{PVPP}) and the active power exchange between the microgrid and the upstream network (P_{slack}) for the 20th of May, while Fig. 6b shows the total reactive power demanded by the microgrid from the upstream network Q_{sl}. The positive values of P_{slack} and Q_{sl} represent active and reactive power imported by the microgrid from the upstream network.

Moreover, only one curve is presented for P_{slack} as largest differences are below 1.2% for all six considered strategies. The average bus voltage values during each time interval and the active power losses are shown in Fig. 6c and Fig. 6d, respectively.

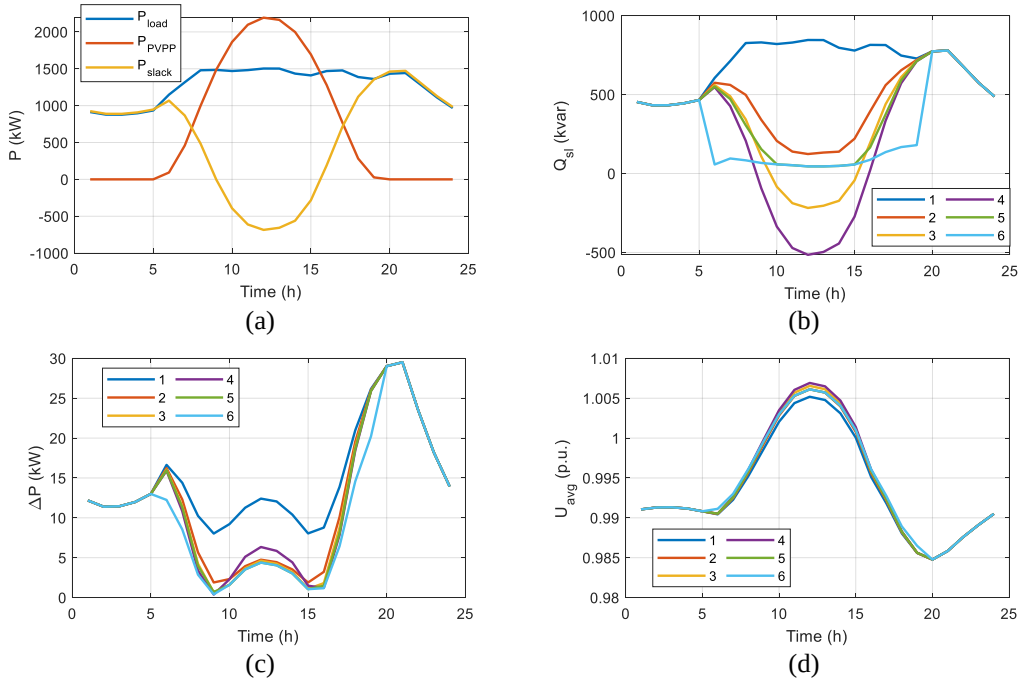

Fig. 6: a) active power balance; b) microgrid reactive power import, c) microgrid active power losses and d) average bus voltage profile.

The results presented in Fig. 6b reveal that the 1st strategy, when the PVPPs operate at unity power factor results in a significant reactive power demand from the upstream network (e.g 845.6 kVAr at the 12th time interval), which is diminished by operating at cosφ = 0.95, according to the 2nd strategy by 85.4% to 123.4 kVAr. The 3rd and 4th strategies provide excess reactive power, which is exported to the upstream network (e.g. –218.1 kVAr and –514.9 kVAr for the 12th interval). On the other hand, by operating the PVPP under the 5th and 6th strategies the reactive power excess is avoided therefore the lowest reactive power exchange between the microgrid, and upstream network is obtained (e.g. 45.3 kVAr for the 12th interval).

The highest active power losses (ΔP) of 12.4 kW during the 12th interval are observed by applying the 1st strategy, as PVPPs operate at unity power factor. The reactive power provided by the PVPPs operated under the 2nd, 3rd, 5th and 6th strategies lead to an approx. 65% active power losses reduction (relative to the 1st strategy), as ΔP values are between 4.4 kW and 4.75 kW during the 12th interval.

However, the excess reactive power provided by the PVPP under the 4th strategy leads to ΔP values of 6.3 kW on the 12th time interval.

The results presented in Fig. 6d reveal that the largest difference between the average bus voltage values is 0.002 p.u. Therefore, the impact of different reactive power control strategies upon the bus voltage profile is insignificant as the microgrid is characterized by a low X/R ratio and relatively short MV electrical line lengths. On the other hand, the line loadings are lowered as the reactive power flow is reduced by the PVPPs reactive power support, leading to a considerable positive impact upon the microgrid active power losses.

4.4. One-year operation analysis

This section presents the impact of different PVPP reactive power control strategies upon the microgrid operation for the duration of an entire year. The first part of this analysis is focused upon the hourly average profile for the reactive power exchange between the microgrid and the upstream network and total microgrid active power losses, presented in Figs. 7a and 7b. In this purpose, each hourly average value is determined by computing the average of all the values recorded on this time interval in all the 365 days within the year.

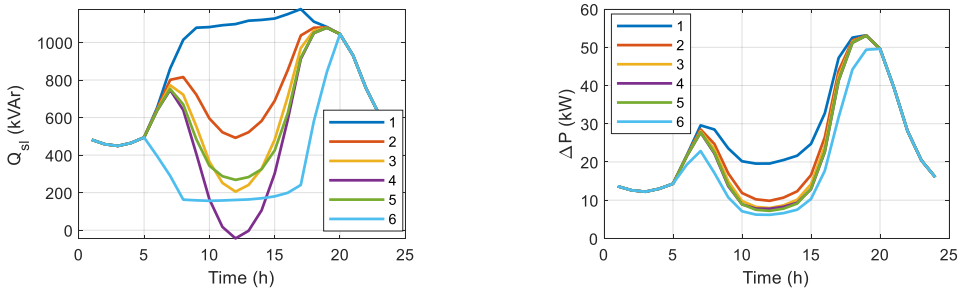

(a) (b)

Fig. 7. Hourly average values for a) microgrid active power losses and b) reactive power import.

When PVPPs operate at unity power factor, in the 1st strategy, the average reactive power demanded by the microgrid from the upstream network Q_{sl} during the 12th time interval is 1178 kVAr. As the power factor is reduced to 0.95, 0.90 and 0.85, the Q_{sl} value on the 12th interval decreases to 491.8 kVAr, 205.3 kVAr and –43.7 kVAr (negative values show that the microgrid exports to the upstream network). The 5th strategy compensates the reactive power demanded by the local loads considering the reactive power limits proportional to P_{gen}, leading to Q_{sl} = 268 kVAr during the 12th interval. The 6th strategy is similar to the 5th with the difference that reactive power limits are extended at partial power. Therefore, the Q_{sl} values from the 8th to 15th time intervals are relative constant between 162 and 180 kVAr. For the 2nd, 3rd, 4th and 5th strategies the PVPP reactive power output

follows the active power output, with a maximum at noon, leading to the so-called "duck curve" observed in Fig. 7a.

The results in Fig. 7b reveal that the 1st strategy produces the largest active power losses, as no reactive power support is provided by the PVPPs. During the noon, the active power losses are reduced by 50%, 60% and 61% by applying the 2nd, 3rd and 4th strategy, consisting in a fixed power factor of 0.95, 0.90 and 0.85 respectively. Furthermore, by using the 5th and 6th strategies the power losses are reduced by 63% and 69% as the reactive power excess is limited by compensating the local loads reactive power demand.

The second part of this analysis is focused on the global impact of different reactive power strategies upon the microgrid operation. In this purpose, the boxplot representation of the reactive power exchange with the upstream network Q_{sl} is shown in Fig. 8, taking into consideration only the day-light hours, when the PVPP generated active power is non-zero. The highest Q_{sl} median value of 1104 kVAr is obtained by applying the 1st strategy when no reactive power support is provided by the PVPPs. For the 2nd, 3rd and 4th strategies, the reactive power support provided at a fixed power factor of 0.95, 0.90 and 0.85 results in a decrease of the Q_{sl} median value to 734 kVAr, 593 kVAr and 473 kVAr respectively. However, these three strategies also provide a reactive power excess, as the minimum values are negative ranging from –188 kVAr to – 938 kVAr, meaning that the microgrid exports reactive power to the upstream network. On the other hand, within the 5th and 6th strategies, the reactive power support is calibrated in order to compensate the local load reactive power demand. In the 5th strategy the reactive power limits are defined by applying the maximum power factor of 0.85 at the generated active power P_{gen}, leading to a Q_{sl} median value of 494 kVAr, while in the 6th strategy, the median value is 155 kVAr, as the maximum power factor is applied at the rated active power P_{max}. For the 5th and 6th strategies the reactive power exported by the microgrid is limited at –51 kVAr, as an adequate reactive power support is provided by the PVPPs avoiding the excess reactive power generation during the mid-day period.

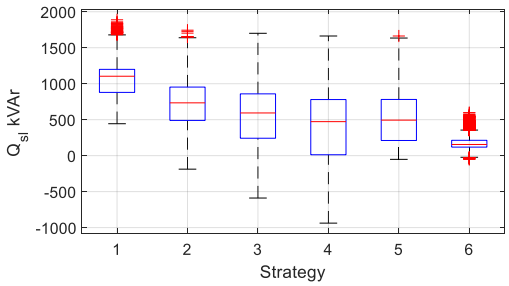

Fig. 8. Boxplot representation of the reactive power exchange with the upstream network.

The yearly average values for bus voltages and active power losses are

presented in Fig. 9a and Fig 9b. The results show that the 1st strategy is the most disadvantageous as the PVPPs do not generate reactive power, leading to the lowest average bus voltage value and highest average active power losses of 26.4 kW. When the PV inverters are also providing reactive power support, the bus voltage values are slightly increased, while the power losses are reduced by 12%, 15%, and 17% for the 2nd, 3rd and 4th strategies. The excess reactive power generated by the PVPPs under the fixed power factor strategies is avoided by applying the local load power factor corrections under the 5th and 6th strategies. The inadequate reactive power support provided under the 4th strategy, lead to slightly higher voltage and power losses values than under the 5th strategy. Finally, the 6th strategy, proves to be the most effective PVPP reactive power control strategy as the extended reactive power limits combined with the local load power factor correction leads to the highest bus voltage values and the lowest active power losses, with 25% lower than in the 1st strategy. It should also be mentioned, that the bus voltage differences are relatively modest as the values are comprised within the [0.9902 p.u ,0.9895 p.u.] interval for all strategies.

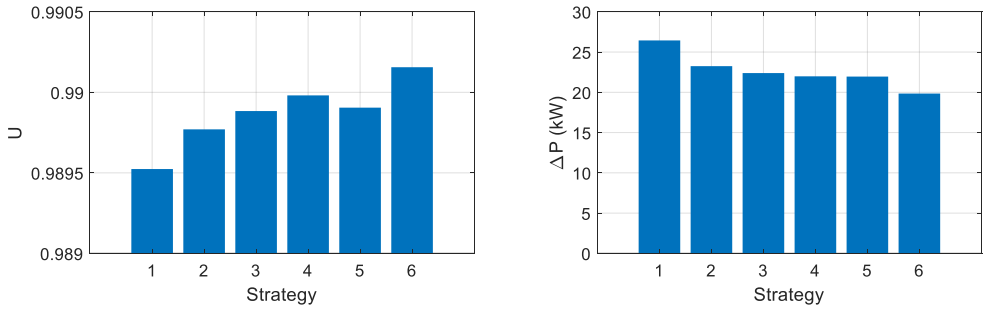

(a) (b)

Fig. 9. Yearly average values for a) bus voltages and b) active power losses.

5. Conclusion

The reactive power control strategies and requirements for medium-size PVPPs are currently updated around the world in order to comply with the new paradigm of increasing renewable energy sources penetration within distribution networks and microgrids. The goal of this paper was to assess six different reactive power control strategies by performing an operational analysis of a microgrid with high PVPP penetration for an entire year with one hour granulation. The results revealed that the initial unity power factor requirement is the most disadvantageous in terms of total microgrid active power losses. An improvement is observed by applying the fixed power factor strategy, limited by the excess reactive power output during PV peak hours. Finally, the best results

are obtained when the PVPPs operate under the local load power factor correction strategy while maintaining the reactive power limits defined at the rated active power at partial power.

REFERENCES

[1]. V. *Tyagi, N. A. Rahim, N. A. Rahim, A. Jeyraj, and L. Selvaraj*, "Progress in solar PV technology: Research and achievement," Renewable and Sustainable Energy Reviews, 20, pp. 443–461, 2013.

[2]. "IEEE Std 2030.7-2017, IEEE Standard for the Specification of Microgrid Controllers".

[3] *K. A. Khan, S. Shafiq, M. Khalid*, "A Strategy for Utilization of Reactive Power Capability of PV Inverters", 9th International Conference on Power and Energy Systems (ICPES), Perth, Australia, 2019.

[4] *H. Li, K. H. Chao, L. L. Li*, "Research on Inverter Integrated Reactive Power Control Strategy in the Grid-Connected PV Systems", Energies, 10(7), pp. 912, 2017.

[5]. *D. O. Sidea, I. I. Picioroaga, C. Bulac*, "Optimal Battery Energy Storage System Scheduling Based on Mutation-Improved Grey Wolf Optimizer Using GPU-Accelerated Load Flow in Active Distribution Networks", IEEE Access, 9, pp. 13922-13937, 2021

[6]. J. *A. M. Rupa and S. Ganesh*, "Power flow analysis for radial distribution system using backward/forward sweep method", World Acad. Sci. Eng. Technol. Int. J. Elect. Comput. Eng., 8(10), pp. 1621-1625, 2014.

[7]. *M. Eremia (ed.) et al.*, "Electric Power Systems: Vol. 1 Electric networks", Publishing House of the Romanian Academy, Bucharest, 2006

[8] *A. Cabrera-Tobar, E. Bullich-Massague, M. Aragues-Penalba, O. Gomis-Bellmunt*, "Active and Reactive Power Control of a PV Generator for Grid Code Compliance", Energies, 12(20), pp. 3872, 2019

[9] *Sandia National Laboratories*, "Reactive Power Capability and Interconnection Requirements for PV and Wind Plants", available on-line at https://www.esig.energy/wiki-main-page/reactive-power-capability-and-interconnection-requirements-for-pv-and-wind-plants/, accessed on 13th of March 2022.

[10] *W. Peng, Y. Baghzouz, S. Haddad*, "Local Load Power Factor Correction by Grid-Interactive PV Inverters", 2013 IEEE Grenoble Conference, Grenoble, France, 2013

[11]. *TF C6.04.02, "*TB 575 Benchmark Systems for Network Integration of Renewable and Distributed Energy Resources", CIGRE, 2014.

[12]. *Twenpower*, "Medium-Voltage XLPE Cables Catalogue", available on-line at: https://t3.lappcdn.com/fileadmin/DAM/Miltronic_Sweden/4_Servicecenter/2Nedladdningscenter/TKF_Twenpower_Medium_Voltage.pdf, accessed on 13th of March 2022.

[13]. *U.S. Department of Energy*, "Simulated Load Profiles for DOE Commercial Reference Buildings (17 Years Using NSRD Data)", on-line: https://openei.org/datasets/dataset/simulated-load-profiles-17year-doe-commercial-reference-buildings, accessed on 13th of March 2022.

[14]. *S. Pfenninger and I. Staffell*, ''Long-term patterns of European PV output using 30 years of validated hourly reanalysis and satellite data,'' Energy, 114, pp. 1251–1265, 2016.

[15]. "MATPOWER User's Manuals", available on-line: https://matpower.org/doc/manuals/, accessed on 13th of March.